Polymer Chemistry

PAPER

Cite this: *Polym. Chem.*, 2016, **7**, 4873

Novel solution-processable functional polyimide/ZrO_2 hybrids with tunable digital memory behaviors†

Chia-Liang Tsai,[a] Tzong-Ming Lee[b] and Guey-Sheng Liou*[a]

Received 13th May 2016,
Accepted 25th June 2016

DOI: 10.1039/c6py00841k

www.rsc.org/polymers

A series of solution-processable sulfur-containing poly(*o*-hydroxy-imide)s **3SOH-RPI** with pendant hydroxyl groups and the corresponding **3SOH-RPI**/ZrO_2 polyimide (PI) hybrids were synthesized from the diamine 3SOH-DA and dianhydrides of CHDA, 6FDA, and DSDA, respectively, for memory application. By introducing acceptors with different electron-withdrawing capabilities (CHDA < 6FDA < DSDA) into polyimide backbones, the obtained polymer memory devices show the memory behaviors of none, DRAM, and SRAM, respectively. In order to facilitate and enhance the memory effects, different amounts of ZrO_2 were incorporated into **3SOH-RPI** to investigate the corresponding memory properties. The hydroxyl groups on the backbone of **3SOH-RPI** could provide reaction sites for organic–inorganic bonding and the homogeneous hybrid thin films could therefore be obtained by controlling the mole ratio of zirconium butoxide/hydroxyl groups *via* a sol–gel reaction. The resulting PI hybrid films displayed electrically programmable digital memory properties from DRAM, SRAM, to WORM with a high ON/OFF current ratio by controlling the content of ZrO_2 from 0 wt% to 30 wt%. Moreover, in order to deeply confirm the memory switching mechanism of **3SOH-RPI/**ZrO_2 hybrids, the devices fabricated both from PI/ZrO_2 and PI/TiO_2 hybrid films were used to demonstrate the effect of LUMO energy levels of ZrO_2 and TiO_2 on the memory characteristics and retention time in this study.

Introduction

In recent years, the use of polymeric materials in optoelectronic devices has attracted significant attention, such as light-emitting devices,[1] transistors,[2] and solar cells,[3] resulting from their advantages of rich structural flexibility, low-cost, solution processability, and three-dimensional stacking capability.[4] Besides, polymeric memory devices have been investigated as a promising alternative to conventional semiconductor-based memory devices. Compared to the traditional inorganic memory materials, polymeric memory materials store information in the form of high (ON) and low (OFF) current states and have the superiority of higher data storage density, longer data retention time, fast speed, and low power consumption.[5]

For resistive type memory materials, electron donor–acceptor polymers are considered as suitable materials because charge transfer (CT) between the donor and acceptor moieties can give rise to a highly conductive state. There have been a number of demonstrations for the application of donor–acceptor polymers in memory devices, such as conjugated polymers,[6] polymers with pendent electroactive chromophores,[7] functional polyimides (PIs),[8] and hybrid composites.[9] Among all the studied donor–acceptor systems, aromatic PIs are promising candidates for memory device applications due to the excellent thermal dimensional stability, chemical resistance, mechanical strength, and high ON/OFF current ratio, resulting from the low conductivity in the OFF state. For example, the non-coplanar electron rich triphenylamine (TPA) with different substituted groups could be introduced into PIs not only to improve the solution processability but also to act as a donor to facilitate the charge transfer (CT) behavior of the related PIs, resulting in diverse memory properties.[10]

Furthermore, CT complex formation could be enhanced by incorporation of supplementary components such as organic molecules or metallic particles into the polymers as electron donors or acceptors.[11] Compared with the polymer memory devices with organic molecules or metallic particles, relatively few studies have been conducted on the polymer memory

[a]*Functional Polymeric Materials Laboratory, Institute of Polymer Science and Engineering, National Taiwan University, 1 Roosevelt Road, 4th Sec., Taipei 10617, Taiwan. E-mail: gsliou@ntu.edu.tw; Fax: +886-2-33665237; Tel: +886-2-33665070*
[b]*Material and Chemical Research Laboratories, Industrial Technology Research Institute, 195 Chung Hsing Road, 4th Sec., Hsinchu 31040, Taiwan*

† Electronic supplementary information (ESI) available: Table: basic properties. Figure: basic properties of hybrids. See DOI: 10.1039/c6py00841k

devices containing semiconducting inorganic particles.[12] Owing to the promising applications in electronic and optoelectronic devices (higher speed and lower power needed), inorganic/organic nanocomposites have attracted researchers' interest.[13] Moreover, due to the advantages of inorganic nanoparticles such as low-cost and ultrahigh-density elements, it is possible to operate several kinds of memory devices to lower power consumption, thus making them a potential candidate for commercializing.[14]

Chemical bond formation based on an *in situ* sol–gel reaction could overcome the agglomeration phenomenon of inorganic nanoparticles by manipulating the organic/inorganic interactions within molecular and nanometer scales. The polyimide/titania (PI/TiO_2) hybrids could tune the memory properties by increasing the TiO_2 content in our previous studies.[15] Moreover, zirconia (ZrO_2) has been demonstrated to have an excellent combination of optical properties, such as a high refraction index, Abbe number, and transparency in a broad spectral range due to the large band gap of ZrO_2 in the range 5.0–5.85 eV,[16] which is larger than TiO_2.

Therefore, a facile *in situ* sol–gel approach was used for obtaining optically transparent polyimide/zirconia (PI/ZrO_2) hybrids in a previous study.[17] Because of the large band gap and the low LUMO energy level, ZrO_2 should be a feasible candidate as an electron acceptor in a PI hybrid system to enhance the optical transparency and increase the retention time by facilitating and stabilizing the CT complex formation of memory devices. Furthermore, compared with conducting supplementary components such as PCBM, CNT, graphene, and metallic particles,[18] the introduction of ZrO_2 could prevent the detriment of the decreasing ON/OFF ratio at high ZrO_2 content due to the low conductivity in the OFF state.

In this study, we therefore designed and synthesized new functional polyimides **3SOH-RPI** from the electron-donating diamine 3SOH-DA and dianhydrides of 6FDA, DSDA, and CHDA, respectively. Besides its higher donor capability, the sulfur-containing **3SOH-RPI** could also be expected to have high dipole moments and lead to stabilization of a high-performance memory device. Furthermore, the corresponding **3SOH-RPI**/ZrO_2 memory devices with different ZrO_2 concentrations were also prepared and investigated systematically to get more insight into the switching mechanism of the **3SOH-RPI**/ZrO_2 memory system, and molecular simulation was also included and is discussed in this study.

Experimental

Materials

4,4′-Bis(4-amino-3-hydroxyphenylthio)diphenyl sulfide (3SOH-DA) was prepared according to a previously reported procedure.[19] 2,2-Bis(3,4-dicarboxyphenyl)hexafluoropropane dianhydride (6FDA) (Chriskev), 3,3′,4,4′-diphenyl sulfone tetracarboxylic dianhydride (DSDA), and 1,2,4,5-cyclohexane tetracarboxylic dianhydride (CHDA) were purified by vacuum sublimation. Tetrabutylammonium perchlorate (TBAP) (Acros) was recrystallized twice with ethyl acetate under a nitrogen atmosphere and then dried *in vacuo* prior to use. All other reagents were used as received from commercial sources.

Polymer synthesis

By using **3SOH-6FPI** as an instance: a stoichiometric mixture of the diamine 3SOH-DA (0.93 g, 2.00 mmol), the dianhydride 6FDA (0.89 g, 2.00 mmol), and a few drops of isoquinoline in *m*-cresol (7 mL) was stirred at ambient temperature under nitrogen for 5 h. Then, the solution was heated to 170–180 °C and maintained at that temperature for 24 h. During this time, the water of imidization was allowed to distill from the reaction mixture along with *m*-cresol. The *m*-cresol was continually replaced so as to keep the total volume of the solution constant. After the solution was allowed to cool to ambient temperature, the viscous solution then was poured slowly into 300 mL of methanol with stirring. The precipitated polymer was collected by filtration, washed thoroughly with hot methanol, and dried under reduced pressure at 150 °C for 15 h. The inherent viscosity of the obtained polyimide **3SOH-6FPI** was 0.51 dL g^{-1} (measured at a concentration of 0.5 g dL^{-1} in DMAc at 30 °C). Yield: 98%.

Preparation of PI/zirconia hybrid films

The synthesis of PI/zirconia hybrid **3S-6FZr30** was used as an example to illustrate the general synthesis route for producing the PI hybrids **3S-6FZrX** (Scheme 1). Firstly, 0.05 g (0.050 mmol) of **3SOH-6FPI** was dissolved in 3 ml of DMAc, and then 0.10 ml of acetic acid was added very slowly into the PI solution and further stirred at room temperature for 30 min. Then, 0.21 ml (0.62 mmol) of $Zr(OBu)_4$ dissolved in 0.21 ml of butanol was added drop-wise by using a syringe into the above solution, and then stirred at room temperature for 30 min. Finally, the resulting precursor solution of **3S-6FZrX** was filtered through a 0.45 mm PTFE filter before being spin-coated onto an ITO glass plate at 1000–2000 rpm

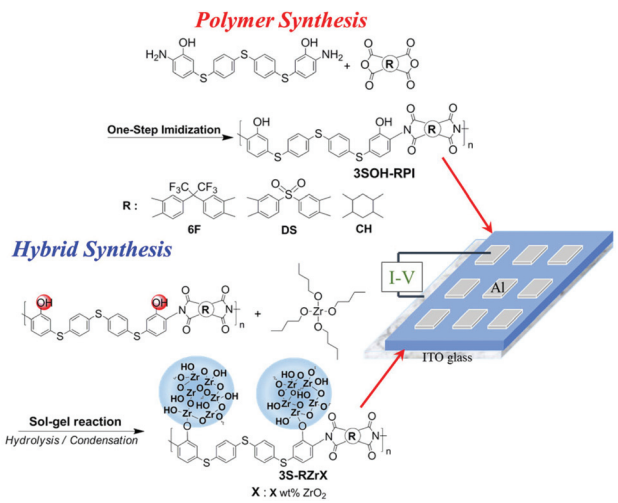

Scheme 1 Synthesis of **3SOH-RPI**, hybrid materials, and schematic diagram of the memory device.

for 60 seconds. The obtained film was treated by the multi-step heating process at 100, 150, and 250 °C for 20 min, and 300 °C for 60 min.

Measurement of basic properties. Fourier transform infrared (FT-IR) spectra were recorded on a Perkin Elmer 100 Model FT-IR spectrometer with a resolution of 1 cm^{-1} and the number of scans is 4. The ^1H NMR spectrum was recorded on a Bruker AC-300 MHz spectrometer in DMSO-d_6, using tetramethylsilane as an internal reference, and peak multiplicity was reported as follows: s, singlet; d, doublet; m, multiplet. The inherent viscosity was determined at 0.5 g dL^{-1} concentration using a Tamson TV-2000 viscometer at 30 °C. Gel permeation chromatographic (GPC) analysis was carried out on a Waters chromatography unit interfaced with a Waters 2410 refractive index detector, calibrated with polystyrene standards. Two Waters 5 μm Styragel HR-2 and HR-4 columns (7.8 mm I. D. × 300 mm) were connected in series with NMP as the eluent at a flow rate of 0.5 ml min^{-1} at 40 °C. Thermogravimetric analysis (TGA) was conducted with TA SDT Q600. Experiments were carried out on approximately 3–5 mg samples heated in flowing nitrogen or air (flow rate = 20 cm^3 min^{-1}) at a heating rate of 20 °C min^{-1}. The coefficient of thermal expansion (CTE) and glass transition temperatures (T_g) are measured on a dilatometer (TA instrument TMA Q400EM). The TMA experiments were conducted from 50 to 380 °C at a scan rate of 10 °C min^{-1} with a tensile probe under an applied constant load of 50 mN. T_g was taken as the onset temperature of probe displacement on the TMA traces. The CTE data were determined in the range of 50–180 °C by using a film-fiber probe in expansion mode. Cyclic voltammetry (CV) was performed with a Bioanalytical System Model CV-27 with the use of a three-electrode cell in which ITO (polymer films area about 0.5 cm × 1.2 cm) was used as a working electrode and a platinum wire as an auxiliary electrode at a scan rate of 100 mV s^{-1} against a Ag/AgCl reference electrode in anhydrous CH_3CN, using 0.1 M of TBAP as a supporting electrolyte. All cell potentials were taken by using a homemade Ag/AgCl, KCl (sat.) reference electrode. The microstructure of the prepared films was examined by using a JOEL JEM-1230 transmission electron microscope (TEM). UV-visible absorption was recorded on a UV-visible spectrophotometer (Hitachi U-4100).

Fabrication and measurement of the memory devices. The memory devices were fabricated with the configuration of ITO/thin film/Al. The ITO glass used for memory devices was precleaned by ultrasonication with water, acetone, and isopropanol each for 15 min. The hybrid thin films were prepared according to a previous procedure using ITO as the substrate. The film thickness was adjusted to be around 50 nm. Finally, a 300 nm-thick Al top electrode was thermally evaporated through a shadow mask (recorded device units of 0.5 × 0.5 mm^2 in size) at a pressure of 10^{-7} Torr with a uniform deposition rate of 3–5 Å s^{-1}. The electrical characterization of the memory device was performed by using a Keithley 4200-SCS semiconductor parameter analyzer equipped with a Keithley 4205-PG2 arbitrary waveform pulse generator. ITO was used as the cathode (maintained as common), and Al was set as the anode during the voltage sweep. The probe tip used 10 μm diameter tungsten wire attached to a tinned copper shaft with a point radius <0.1 μm (GGB Industries, Inc.).

Molecular simulation. Molecular simulation in this study was carried out with the Gaussian 09 program package. The equilibrium ground state geometry and electronic properties of the basic unit of these aromatic PIs were optimized by means of the density functional theory (DFT) method at the B3LYP level of theory (Beckesstyle three-parameter density functional theory using the Lee–Yang–Parr correlation functional) with the 6-31G(d) basis set.

Results and discussion

Basic characterization

3SOH-6FPI, **3SOH-DSPI** and **3SOH-CHPI** were synthesized by the one-step method starting from the hydroxyl-containing diamine monomer **3SOH-DA** and aromatic or aliphatic tetracarboxylic dianhydrides (**6FDA** and **DSDA**, **CHDA**) in the presence of a catalytic amount of isoquinoline at 170–180 °C as shown in Scheme 1. The polymerization proceeded homogeneously throughout the procedure, and afforded clear and viscous polymer solutions in high yields. All the polymers precipitated in a fiber-like form when the resulting polymer solutions were slowly poured into methanol. The inherent viscosities (η_{inh}), weight average molecular weights (M_w), and the polydispersity index (PDI) of the obtained PIs are listed in Table S1.† The formation of **3SOH-RPI** was confirmed by FTIR and NMR measurements. The FTIR spectrum of **3SOH-6FPI** (film) exhibited broad absorption bands in the region of 2500 to 3700 cm^{-1} (O–H stretch) and characteristic imide absorption bands at 1785 (asymmetrical C═O), 1722 (symmetrical C═O), 1390 (C–N), 1105 (Ar–S–Ar), 1256 (C–F), and 748 cm^{-1} (imide ring deformation) (Fig. S1a†). **3SOH-DSPI** (film) exhibited broad absorption bands in the region of 2750 to 3300 cm^{-1} (O–H stretch) and characteristic imide absorption bands at 1783 (asymmetrical C═O), 1721 (symmetrical C═O), 1390 (C–N), 1102 (Ar–S–Ar), and 748 cm^{-1} (imide ring deformation) (Fig. S1c†). **3SOH-CHPI** (film) showed broad absorption bands in the region of 2750 to 3500 cm^{-1} (O–H stretch) and characteristic imide absorption bands at 1783 (asymmetrical C═O), 1721 (symmetrical C═O), 1395 (C–N), 1101 (Ar–S–Ar) and 745 cm^{-1} (imide ring deformation) (Fig. S1e†). The ^1H NMR result of **3SOH-6FPI** (DMSO-d_6, δ, ppm): 6.80 (m, 4H), 7.33 (m, 10H), 7.71 (s, 2H), 7.91 (d, 2H), 8.10 (d, 2H) and 10.08 (s, 2H, OH). **3SOH-DSPI** (DMSO-d_6, δ, ppm): 6.80 (m, 4H), 7.40 (m, 10H), 8.20 (d, 2H), 8.60 (d, 2H) and 10.09 (s, 2H, OH). **3SOH-CHPI** (DMSO-d_6, δ, ppm): 2.20 (q, 4H), 2.70 (t, 4H) 6.80 (m, 4H), 7.20–7.60 (m, 12H), 7.70 (d, 2H) and 10.02 (s, 2H, OH). **3SOH-RPI** exhibited high solubility in common organic solvents which is beneficial for solution-processing in memory device applications (Table S2†).

Thermal behaviors of the obtained **3SOH-RPI**/ZrO_2 hybrids evaluated by TGA and TMA are summarized in Table S3.† The typical TGA curves (Fig. S2†) of **3S-6FZrX** displayed excellent

thermal stability up to 400 °C both in nitrogen and air, and the carbonized residue (char yield) increased with the increasing zirconia content. The zirconia contents in the PI hybrids estimated by using the char yields in air flow matched with the theoretical calculation, confirming successful incorporation of the zirconia. The typical TMA thermograms of **3SOH-6FPI** and the corresponding PI hybrids indicated that the glass transition temperature (T_g) could be increased from 230 °C to 287 °C with the increasing zirconia content (Fig. S3†). Meanwhile, the coefficient of thermal expansion (CTE) of the pristine PIs and their PI/ZrO_2 hybrid films is summarized in Table S3,† and the reinforced hybrids reveal much lower CTE values than pristine PIs, and decrease with the increasing volume fraction of inorganic reinforcement.

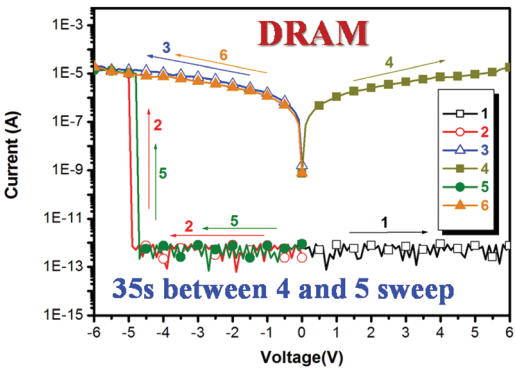

Fig. 1 Current–voltage (*I–V*) characteristics of the ITO/**3SOH-6FPI** hybrid materials/Al memory device.

Absorption and electrochemistry

The UV-vis absorption spectra of **3SOH-RPI** and the onset wavelength of optical absorption were utilized to obtain the optical energy band gap (E_g) of the PIs (Fig. S4†). The electrochemical properties of **3SOH-RPI** were investigated by cyclic voltammetry (CV) (Fig. S5†) conducted with the cast films on an ITO-coated glass slide as the working electrode in anhydrous acetonitrile (CH_3CN), using 0.1 M of TBAP as a supporting electrolyte. The redox potentials of the PIs as well as their respective highest occupied molecular orbital (HOMO) and lowest unoccupied molecular orbital (LUMO) (*versus* vacuum) were calculated and are summarized in Table 1. The onset oxidation of **3SOH-6FPI** exhibited at 1.11 V. The HOMO levels also called ionization potentials (*versus* vacuum) of **3SOH-6FPI** could be estimated from the onset of their oxidation in CV experiments as 5.55 eV (on the basis that ferrocene/ferrocenium is 4.8 eV below the vacuum level with E_{onset} = 0.36 V).

Memory device characteristics

The memory behavior of **3SOH-RPI** and **3SOH-RPI**/ZrO_2 hybrids was depicted by using the current–voltage (*I–V*) characteristics of an ITO/polymer/Al sandwich device as shown in Scheme 1. Within the sandwich device, a polymer or hybrid film was used as an active layer between Al and ITO as the top and bottom electrodes. To exclude the effect of the polymer film thickness on memory properties, a standard thickness (50 nm) was used without specific mention. Fig. 1 shows the *I–V* result of **3SOH-6FPI**, which was measured with a compliance current of 0.01 A. During the first positive sweep from 0 V to 6 V, the device stayed in the low-conductivity (OFF) state in a current range of 10^{-12}–10^{-13} A, which means that the positive applied voltage could not switch the memory device on. In contrast, the current increased abruptly from 10^{-12}–10^{-13} to 10^{-5} A (high-conductivity state) at the threshold voltage of −4.9 V in the second negative sweep, indicating the transition from the OFF state to the high-conductivity (ON) state. In a memory device, this OFF-to-ON transition can be defined as a "writing" process. The device remained in the ON state during the subsequent negative scan (the third sweep) and then positive scan (the fourth sweep). The fifth sweep was conducted after turning off the power for about 35 seconds, and found that the ON state had relaxed to the steady OFF state. It suggests that the ON state could be retained for a short period of time after the removal of applied voltage and then relaxed to the initial OFF state eventually. The device could also be reprogrammed by starting from the OFF state to the ON state again with an accurate threshold voltage of −4.7 V in the fifth sweep, and kept in the ON state in the subsequent sixth sweep. The short retention time of the ON state indicates that the memory device of **3SOH-6FPI** has a volatile DRAM (Dynamic Random Access Memory) property.

In order to explore the transition from DRAM to SRAM (Static Random Access Memory) (6 minutes) by introducing 7 wt% ZrO_2 into **3SOH-6FPI**, the intermediate **3S-6FZr5** hybrid films were prepared to fabricate the sandwich devices for investigating the electrical characteristics. Both DRAM and

Table 1 Electrochemical and optical properties of **3SOH-RPI**

Polymer	UV-vis absorption (nm)		Oxidation potential (V) (*vs.* Ag/AgCl in CH_3CN)	E_g[a] (eV)	HOMO[b] (eV)	LUMO (eV)
	λ_{max}	λ_{onset}	E_{onset}			
3SOH-6FPI	305	343	1.11	3.61	5.55	1.94
3SOH-DSPI	313	365	1.27	3.39	5.71	2.32
3SOH-CHPI	293	331	1.16	3.75	5.60	1.85

[a] The data were calculated from polymer films by using the equation: $E_g = 1240/\lambda_{onset}$ (energy gap between the HOMO and the LUMO). [b] The HOMO energy levels were calculated from CV and were referenced to ferrocene (4.8 eV; onset = 0.36 V).

SRAM properties were present in the devices of **3S-6FZr5**. The probability of the resulting DRAM and SRAM characteristics of **3S-6FZr5** was 70% for DRAM and 30% for SRAM, respectively (Fig. 2a and b), while the SRAM behavior of **3S-6FZr5** only possessed a 2 minute retention time. Fig. 2c depicts the *I–V* result of **3S-6FZr7**. A sharp increase of the current could be observed at −4.5 V during the second negative sweep. The device of **3S-6FZr7** maintained the ON state after turning off the power for a longer period of time than **3SOH-6FPI**. The fifth sweep was conducted after turning off the power for about 6 minutes and the device could be switched to the ON state again at the threshold voltage of −4.2 V. The longer retention time in the ON state yet volatile, as well as the randomly accessible ON and OFF states is similar to the behavior of SRAM.

Fig. 3 depicts the memory results of the PI hybrids **3S-6FZr30** and **3S-6FTi30**, respectively. Compared to the volatile DRAM and SRAM properties, the ON state of **3S-6FZr30** and **3S-6FTi30** could be maintained even after turning off the power for 3 hours or a longer time since it has been switched on. Thus, this *I–V* characteristic indicates that the memory devices based on **3S-6FZr30** and **3S-6FTi30** hybrid films revealed the non-volatile write-once-read-many (WORM) memory property. Furthermore, the devices derived from the PI hybrid film **3S-6FTi30** with higher (30 wt%) TiO_2 could also be switched to the ON state by the positive voltage at 2.9 V, while the PI hybrid film **3S-6FZr30** with the same 30 wt% ZrO_2 only could be switched to the ON state by the negative voltage. Even at the scanning voltage of up to 10 V, the device still remained in the OFF state (Fig. 3b).

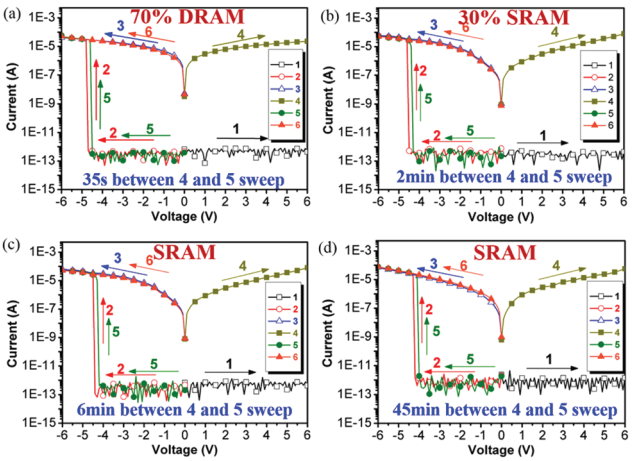

Fig. 2 Current–voltage (*I–V*) characteristics of the ITO/hybrid materials/Al memory device (a), (b) **3S-6FZr5**, (c) **3S-6FZr7** and (d) **3S-6FZr10**.

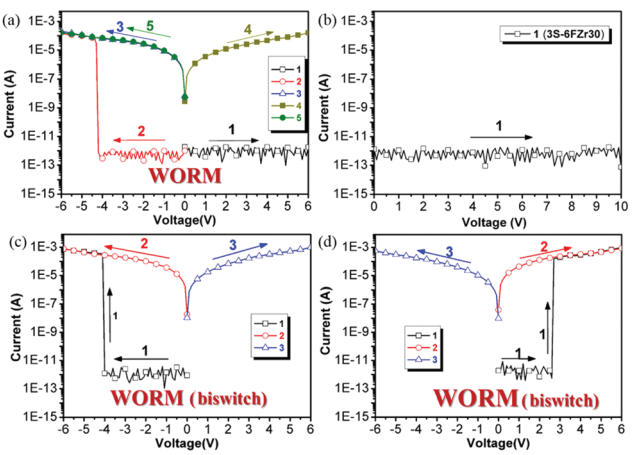

Fig. 3 Current–voltage (*I–V*) characteristics of the ITO/hybrid materials/Al memory device (a) and (b) **3S-6FZr30**, (c) and (d) **3S-6FTi30**.

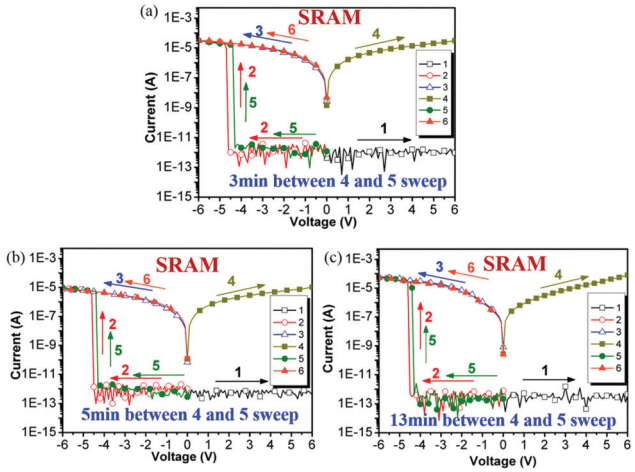

Fig. 4 Current–voltage (*I–V*) characteristics of the ITO/hybrid materials/Al memory device (a) **3SOH-DSPI**, (b) **3S-DSZr5** and (c) **3S-DSZr7**.

In addition, the *I–V* result of **3SOH-DSPI** with a stronger electron-withdrawing ability of the acceptor shown in Fig. 4 reveals the volatile SRAM property, displaying a longer retention time than the case of **3SOH-6FPI**. Moreover, the semi-aromatic PI **3SOH-CHPI** did not show any memory property because there is an absence of the electron-withdrawing moiety for stabilizing the charge transfer. However, the increase in the electron acceptor ZrO_2 content (0–30 wt%) of **3S-CHZrX** hybrids resulted in a longer retention time gradually with memory properties from none to DRAM, SRAM, and WORM, respectively (Fig. 5). Generally, the memory device reveals a longer retention time with the increasing content of ZrO_2, but the PI/ZrO_2 hybrid system only could be switched to the ON state by applying a negative voltage compared with the TiO_2 hybrid system. The memory properties of **3SOH-RPI** hybrid materials with different ZrO_2 and TiO_2 contents from 0 wt% to 30 wt% are summarized in Fig. 6.

Switching mechanism

In order to get more insight into the memory behavior of the polyimide 3SOH-6FPI, molecular simulation on the basic unit was carried out by using DFT/B3LYP/6-31G(d) with the Gaussian 09 program as shown in Fig. 7. Furthermore, the HOMO of **3SOH-6FPI** is located mainly at the electron-donating sulfur-containing diamine moiety, while LUMOs are distributed around electron-withdrawing phthalimide units, the adjacent

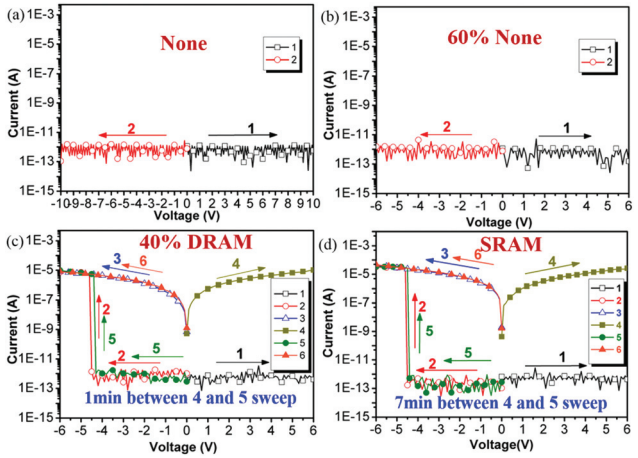

Fig. 5 Current–voltage (*I*–*V*) characteristics of the ITO/hybrid materials/Al memory device (a) **3SOH-CHPI**, (b), (c) **3S-CHZr5** and (d) **3S-CHZr7**.

Amounts of acceptor increase

PI+ZrO_2 or TiO_2 hybrid	0wt%	5wt%	7wt%	10wt%	30wt%
3S-6FZrX	DRAM (35sec)	70% DRAM/ 30% SRAM (2min)	SRAM (6min)	SRAM (45min)	WORM
3S-6FTiX	DRAM (35sec)	50% DRAM/ 50% SRAM (2min)	SRAM (7min)	SRAM (95min)	WORM (biswitch)
3S-CHZrX	None	60% None/ 40% DRAM (1min)	SRAM (4min)	SRAM (15min)	WORM
3S-DSZrX	SRAM (3min)	SRAM (5min)	SRAM (13min)	SRAM (75min)	WORM

Fig. 6 Memory properties of **3SOH-RPI** hybrid materials.

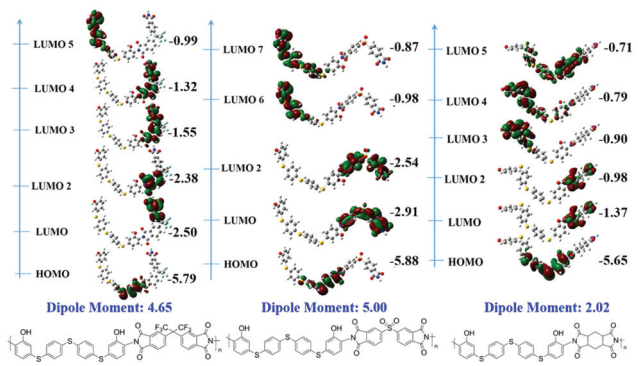

Fig. 7 Calculated molecular orbitals and corresponding energy levels of the basic units of **3SOH-RPI**.

phenyl ring, and the hexafluoroisopropylidene group. According to previous literature,[20] when the applied electric field reached the switching-on voltage, some electrons at the HOMO accumulate energy and transit to the LUMO to form a CT complex (ON state) by different ways. When the intra- or intermolecular CT occurred by the applied electric field, the generating holes can be delocalized to the sulfur-containing diamine moieties forming an open channel in the HOMO of PIs for the charge carriers (holes) to migrate through. Thus, when the negative sweep was conducted, the hole could be injected from the bottom electrode ITO to the HOMO of the polymer due to the lower band gap between ITO (−4.8 eV) and the HOMO of the polymer as shown in Fig. 8. In contrast, during a positive sweep, a hole is difficult to be injected from the top electrode Al into the HOMO of the polymer because of the larger energy gap between the work function of Al (−4.2 eV) and the HOMO of the polymer, thus the memory device could not be switched to the ON state. However, with the introduction of TiO_2 into **3SOH-6FPI**, the hybrid materials therefore have a lower LUMO energy level and could be switched to the ON state at positive sweep. This phenomenon could be attributed to the smaller band gap between the LUMO of TiO_2 (−4.2 eV) and the work function of Al (−4.2 eV) and ITO (−4.8 V).

However, with the introduction of ZrO_2 into **3SOH-6FPI**, the hybrid materials could not be switched to the ON state by positive sweep due to the higher LUMO energy level than TiO_2 and a larger band gap between the LUMO of ZrO_2 (−3.32 eV) and the work function of Al (−4.2 eV) and ITO (−4.8 V). In addition to the switching-on voltage, introduction of ZrO_2 as electron acceptors into **3SOH-RPI** could also stabilize the charge transfer complex and thus **3SOH-6FPI**/ZrO_2 hybrid materials with higher ZrO_2 contents revealed a longer retention time. Furthermore, because of the different band gaps between the LUMO and the work function of Al, the charge transfer complexes of the **3S-6FZrX** hybrid system are less stable, thus **3S-6FZrX** hybrid materials revealed a shorter retention time than the corresponding **3S-6FTiX** hybrid system.

TEM was also used to characterize the morphology of the prepared hybrid films as shown in Fig. 9. The dark regions indicate the formation of ZrO_2 clusters with a domain size of around 6 nm which were well dispersed in the matrix of **3SOH-6FPI** even at 30 wt% ZrO_2 content. Compared to previous literature,[21] the PI hybrid films prepared in this study display much better nano-scale distribution of ZiO_2, and could afford excellent film quality to avoid filament formation. Besides, the obtained PI hybrids with a higher amount of ZrO_2 and a very small domain size within the matrix of **3SOH-6FPI** could facilitate and stabilize the charge separation state, hin-

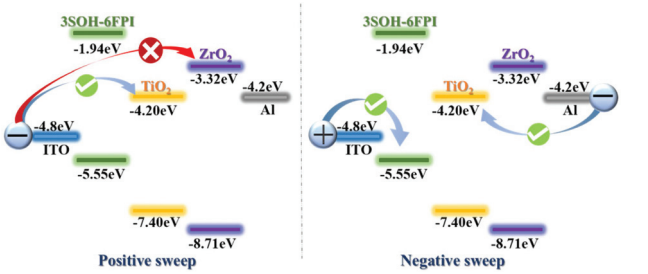

Fig. 8 HOMO and LUMO energy levels of **3SOH-6FPI**, ZrO_2 and TiO_2 along with the work function of the electrodes.

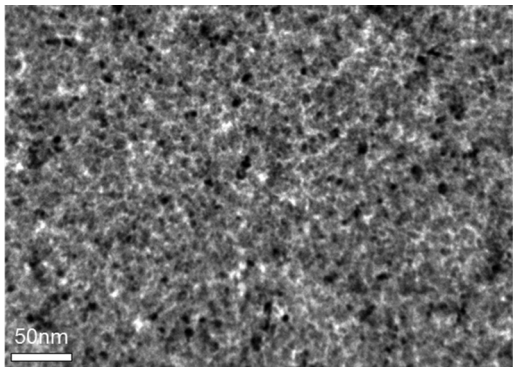

Fig. 9 TEM image of the hybrid material **3S-6FZr30**.

dering back recombination even under the reverse bias. Thus, the high conductance state can be retained for a much longer time, tuning the devices from DRAM to SRAM, and even with WORM type memory characteristics. Furthermore, the high ON/OFF ratio of these hybrid materials could be maintained even at high ZrO_2 content due to the insulator behavior of ZrO_2, resulting in low conductivity in the OFF state.

Conclusion

A series of solution-processable sulfur-containing polyimides **3SOH-RPI** with pendant hydroxyl groups were synthesized and used for memory application with the introduction of ZrO_2. The hydroxyl groups on the backbone of **3SOH-RPI** provide reaction sites for organic–inorganic bonding and the homogeneous hybrid thin films were therefore obtained. The resulting hybrid films with different ZrO_2 contents from 0 wt% to 30 wt% exhibited tunable memory properties from DRAM, SRAM, to WORM with a high ON/OFF current ratio (10^8). Furthermore, the higher TiO_2 containing hybrid film **3S-6FTi30** also could be switched to the ON state by the positive voltage, but the higher ZrO_2 containing hybrid film **3S-6FZr30** could be switched to the ON state only by the negative voltage. Molecular simulation and the electrode effect are also discussed to understand the switching mechanism of **3SOH-RPI**/ZrO_2.

Acknowledgements

The authors gratefully acknowledge the Ministry of Science and Technology of Taiwan for the financial support.

References

1 (*a*) R. H. Friend, R. W. Gymer, A. B. Holmes, J. H. Burroughes, R. N. Marks, C. Taliani, D. D. C. Bradley, D. A. Dos Santos, J. L. Bredas, M. Logdlund and W. R. Salaneck, *Nature*, 1999, **397**, 121; (*b*) Q. Peng, E. T. Kang, K. G. Neoh, D. Xiaob and D. Zou, *J. Mater. Chem.*, 2006, **16**, 376; (*c*) Y. Shao, X. Gong, A. J. Heeger, M. Liu and A. K. Y. Jen, *Adv. Mater.*, 2009, **21**, 1972.

2 (*a*) H. Yan, Z. H. Chen, Y. Zheng, C. Newman, J. R. Quinn, F. Dotz, M. Kastler and A. Facchetti, *Nature*, 2009, **457**, 679; (*b*) Y. H. Chou, H. J. Yen, C. L. Tsai, W. Y. Lee, G. S. Liou and W. C. Chen, *J. Mater. Chem. C*, 2013, **1**, 3235.

3 (*a*) G. Yu, J. Gao, J. C. Hummelen, F. Wudl and A. J. Heeger, *Science*, 1995, **270**, 1789; (*b*) C. J. Brabec, N. S. Sariciftci and J. C. Hummelen, *Adv. Funct. Mater.*, 2001, **11**, 15; (*c*) M. H. Chen, J. Hou, Z. Hong, G. Yang, S. Sista, L. M. Chen and Y. Yang, *Adv. Mater.*, 2009, **21**, 4238.

4 A. Stikeman, *Technol. Rev.*, 2002, **105**, 31.

5 (*a*) H. Gruber, *Resour. Policy*, 2000, **29**, 725; (*b*) S. Moller, C. Perlov, W. Jackson, C. Taussig and S. R. Forrest, *Nature*, 2003, **426**, 166.

6 (*a*) X. D. Zhuang, Y. Chen, G. Liu, P. P. Li, C. X. Zhu, E. T. Kang, K. G. Noeh, B. Zhang, J. H. Zhu and Y. X. Li, *Adv. Mater.*, 2010, **22**, 1731; (*b*) X. D. Zhuang, Y. Chen, B. X. Li, D. G. Ma, B. Zhang and Y. Li, *Chem. Mater.*, 2010, **22**, 4455; (*c*) S. J. Liu, W. P. Lin, M. D. Yi, W. J. Xu, C. Tang, Q. Zhao, S. H. Ye, X. M. Liu and W. Huang, *J. Mater. Chem.*, 2012, **22**, 22964; (*d*) S. Baek, D. Lee, J. Kim, S. H. Hong, O. Kim and M. Ree, *Adv. Funct. Mater.*, 2007, **17**, 2637; (*e*) H. C. Wu, A. D. Yu, W. Y. Lee, C. L. Liu and W. C. Chen, *Chem. Commun.*, 2012, **48**, 9135; (*f*) F. L. Ye, P. Y. Gu, F. Zhou, H. F. Liu, X. P. Xu, H. Li, Q. F. Xu and J. Lu, *Polymer*, 2013, **54**, 3324; (*g*) D. Wang, H. Li, N. Li, Y. Zhao, Q. Zhou, Q. Xu, J. Lu and L. Wang, *Mater. Chem. Phys.*, 2012, **134**, 273.

7 (*a*) B. Zhang, G. Liu, Y. Chen, C. Wang, K. G. Neoh, T. Bai and E. T. Kang, *ChemPlusChem*, 2012, **77**, 74; (*b*) S. J. Liu, P. Wang, Q. Zhao, H. Y. Yang, J. Wong, H. B. Sun, X. C. Dong, W. P. Lin and W. Huang, *Adv. Mater.*, 2012, **24**, 2901; (*c*) S. G. Hahm, N. G. Kang, W. Kwon, K. Kim, Y. K. Ko, S. Ahn, B. G. Kang, T. Chang, J. S. Lee and M. Ree, *Adv. Mater.*, 2012, **24**, 1062; (*d*) H. Zhuang, X. Xu, Y. Liu, Q. Zhou, X. Xu, H. Li, Q. Xu, N. Li, J. Lu and L. Wang, *J. Phys. Chem. C*, 2012, **116**, 25546; (*e*) Y. Liu, N. Li, X. Xia, J. Ge, Q. Xu and J. Lu, *Eur. Polym. J.*, 2011, **47**, 1160; (*f*) J. Liu, P. Gu, F. Zhou, Q. Xu, J. Lu, H. Li and L. Wang, *J. Mater. Chem. C*, 2013, **1**, 3947; (*g*) D. He, H. Zhuang, H. Zhuang, H. Liu, H. Liu, H. Li and J. Lu, *J. Mater. Chem. C*, 2013, **1**, 7883; (*h*) L. Shi, H. Ye, W. Liu, G. Tian, S. Qi and D. Wu, *J. Mater. Chem. C*, 2013, **1**, 7887.

8 (*a*) T. Kurosawa, Y. C. Lai, T. Higashihara, M. Ueda, C. L. Liu and W. C. Chen, *Macromolecules*, 2012, **45**, 4556; (*b*) F. Chen, G. Tian, L. Shi, S. Qi and D. Wu, *RSC Adv.*, 2012, **2**, 12879; (*c*) Y. Liu, Y. Zhang, Q. Lan, S. Liu, Z. Qin, L. Chen, C. Zhao, Z. Chi, J. Xu and J. Economy, *Chem. Mater.*, 2012, **24**, 1212; (*d*) S. G. Hahm, S. Choi, S. H. Hong, T. J. Lee, S. Park, D. M. Kim, W. S. Kwon, K. Kim, O. Kim and M. Ree, *Adv. Funct. Mater.*, 2008, **18**, 3276; (*e*) Q. Liu, K. Jiang, Y. Wen, J. Wang, J. Luo and Y. Song, *Appl. Phys. Lett.*, 2010, **97**, 253304; (*f*) Y. Li, Y. Chu, R. Fang, S. Ding, Y. Wang, Y. Shen and A. Zheng, *Polymer*, 2012, **53**, 229;

(*g*) G. Tian, S. Qi, F. Chen, L. Shi, W. Hu and D. Wu, *Appl. Phys. Lett.*, 2011, **98**, 203302; (*h*) L. Shi, H. Ye, W. Liu, G. Tian, S. Qi and D. Wu, *J. Mater. Chem. C*, 2013, **1**, 7387; (*i*) N. H. You, C. C. Chueh, C. L. Liu, M. Ueda and W. C. Chen, *Macromolecules*, 2009, **42**, 4456.

9 (*a*) D. B. Velusamy, S. K. Hwang, R. H. Kim, G. Song, S. H. Cho, I. Bae and C. Park, *J. Mater. Chem.*, 2012, **22**, 25183; (*b*) M. A. Khan, U. S. Bhansali, D. Cha and H. N. Alshareef, *Adv. Funct. Mater.*, 2013, **23**, 2145; (*c*) S. Gao, C. Song, C. Chen, F. Zeng and F. Pan, *J. Phys. Chem. C*, 2012, **116**, 17955; (*d*) C. J. Chen, Y. C. Hu and G. S. Liou, *Chem. Commun.*, 2013, **49**, 2804; (*e*) L. Q. Xu, B. Zhang, K. G. Neoh, E. T. Kang and G. D. Fu, *Macromol. Rapid Commun.*, 2013, **34**, 234; (*f*) M. A. Mamo, A. O. Sustaita, N. J. Coville and I. A. Hummelgen, *Org. Electron.*, 2013, **14**, 175.

10 (*a*) C. J. Chen, H. J. Yen, W. C. Chen and G. S. Liou, *J. Mater. Chem.*, 2012, **22**, 14085; (*b*) T. J. Lee, C. W. Chang, S. G. Hahm, K. Kim, S. Park, D. M. Kim, J. Kim, W. S. Kwon, G. S. Liou and M. Ree, *Nanotechnology*, 2009, **20**, 135204–135201; (*c*) K. Kim, H. J. Yen, Y. G. Ko, C. W. Chang, W. Kwon, G. S. Liou and M. Ree, *Polymer*, 2012, **53**, 4135; (*d*) Y. G. Ko, W. Kwon, H. J. Yen, C. W. Chang, D. M. Kim, K. Kim, S. G. Hahm, T. J. Lee, G. S. Liou and M. Ree, *Macromolecules*, 2012, **45**, 3749; (*e*) Y. L. Liu, K. L. Wang, G. S. Huang, C. X. Zhu, E. S. Tok, K. G. Neoh and E. T. Kang, *Chem. Mater.*, 2009, **21**, 3391; (*f*) T. J. Lee, Y. G. Ko, H. J. Yen, K. Kim, D. M. Kim, W. Kwon, S. G. Hahm, G. S. Liou and M. Ree, *Polym. Chem.*, 2012, **3**, 1276; (*g*) A. D. Yu, T. Kurosawa, Y. C. Lai, T. Higashihara, M. Ueda, C. L. Liu and W. C. Chen, *J. Mater. Chem.*, 2012, **22**, 20754; (*h*) H. J. Yen, C. J. Chen and G. S. Liou, *Adv. Funct. Mater.*, 2013, **23**, 5307.

11 (*a*) J. Ouyang, C. W. Chu, C. R. Szmanda, L. Ma and Y. Yang, *Nat. Mater.*, 2004, **3**, 918; (*b*) R. J. Tseng, J. Huang, J. Quyang, R. B. Kaner and Y. Yang, *Nano Lett.*, 2005, **5**, 1077.

12 F. Li, T. W. Kim, W. Dong and Y. H. Kim, *Appl. Phys. Lett.*, 2008, **92**, 011906.

13 (*a*) N. J. Craig, J. M. Taylor, E. A. Lester, C. M. Marcus, M. P. Hanson and A. C. Gossard, *Science*, 2004, **304**, 565; (*b*) S. Coe, W.-K. Woo, M. Bawendi and V. Bulovic, *Nature*, 2002, **420**, 800; (*c*) M. Kroutvar, Y. Ducommun, D. Heiss, M. Bichler, D. Schuh, G. Abstreiter and J. J. Finley, *Nature*, 2004, **432**, 81.

14 (*a*) E. Kapetanakis, P. Normand, D. Tsoukalas and K. Beltsios, *Appl. Phys. Lett.*, 2002, **80**, 2794; (*b*) M. Perego, S. Ferrari, M. Fanciulli, G. B. Assayag, C. Bonafos, M. Carrada and A. Claverie, *J. Appl. Phys.*, 2004, **95**, 257.

15 C. J. Chen, C. L. Tsai and G. S. Liou, *J. Mater. Chem. C*, 2014, **2**, 2842.

16 (*a*) M. Zelner, H. Minti, R. Reisfeld, H. Cohen and R. Tenne, *Chem. Mater.*, 1997, **9**, 2541; (*b*) A. Sashchiuk, E. Lifshitz, R. Reisfeld, T. Saraidarov, M. Zelner and A. Willenz, *J. Sol–Gel Sci. Technol.*, 2002, **24**, 31; (*c*) M. T. Wang, T. H. Wang and J. Lee, *Microelectron. Reliab.*, 2005, **45**, 969.

17 C. L. Tsai and G. S. Liou, *Chem. Commun.*, 2015, **51**, 13523.

18 C. J. Chen, Y. C. Hu and G. S. Liou, *Chem. Commun.*, 2013, **49**, 2804.

19 H. J. Yen, C. L. Tsai, P. H. Wang and G. S. Liou, *RSC Adv.*, 2013, **3**, 17048.

20 Q. D. Ling, F. C. Chang, Y. Song, C. X. Zhu, D. J. Liaw, D. S. H. Chan, E. T. Kang and K. G. Neoh, *J. Am. Chem. Soc.*, 2006, **128**, 8732.

21 B. Cho, T. W. Kim, M. Choe, G. Wang, S. Song and T. Lee, *Org. Electron.*, 2009, **10**, 473.

